International Scientific Colloquium
Modelling for Electromagnetic Processing
Hannover, October 27-29, 2008

Crossed EM Fields Driven Weak Conducting Flow in Annular Cylinder

A. Jakovics, V. Geza, B. Halbedel

Abstract

Numerical investigation of new equipment for electromagnetic processing of weak conducting material melts was carried on. Significance of different effects and physical phenomena was evaluated, including previously neglected heat transfer and buoyancy effects.

1. General information

The liquid melt EM driven flow is widely investigated, because it can be used in various industry applications, especially in metallurgic and semiconductor material technologies, where melts has high conductivity ($\sigma>10^5$ S/m). However, for some technological objectives, EM impact can be used even for weak conducting (σ=1...100 S/m) oxides and glass-like materials.

In earlier paper [1] two different electromagnetic (EM) source driven weak conducting melt flow between coaxial shells was studied. Not all important physical effects were included in that phase of investigation.

The aim of this paper is to determine influence of EM field on weak conducting melt flow, estimate role of different effects, including previously neglected phenomena – heat transfer, buoyancy effects. No experimental device is built yet, so we were free to *play* with parameters in wide range and parameter and geometry optimization was not the task at this stage of investigation.

2. Investigated equipment

Investigation object is molten glass with high viscosity (η=1...100 Pa·s) that is located between coaxial metallic (e.g. platinum) shields ($\sigma_{shell}=2\cdot10^6$ S/m), these shields have alternating voltage applied, and all this system is surrounded by coaxial inductors. (figure 1.) In this situation the melt is affected by "crossed" EM fields from two sources – induction effects (currents in azimuthal direction), which are generated by alternating current (AC) flowing in inductors, and currents flowing in melt in the radial direction which is result of potential difference applied to metallic shells. Applied voltage has same frequency as current in inductors.

Due to the interaction of both processes, additional Lorentz force density components appear if compared to classical cylindrical induction furnace, where is no applied voltage [2].

Tab. 1. Geometry parameter for modelled equipment

Inner shell outer radius, *mm*	10.0
Outer shell outer radius, *mm*	20.0
Inductor radius, *mm*	30.0
Thickness of shells, *mm*	1.2
Vertical distance between coils, *mm*	30.0

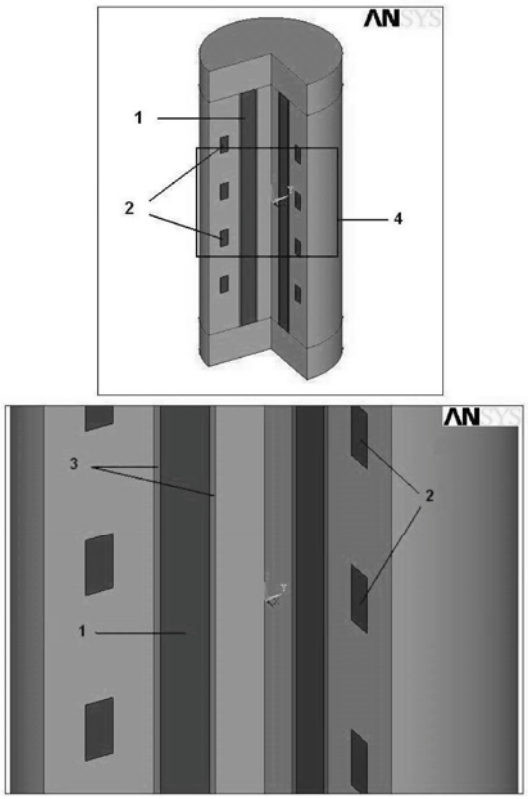

Fig. 1. Scheme of modeled equipment and cut-out. (1 – liquid melt, 2 – coils, 3 – concentric metallic shell, 4 – cut-out region)

Joule heat generation in melt and shells creates temperature gradient appears and additional buoyancy force acts on melt.

See table 1 for equipment geometry and table 2 for typical parameters.

However, there are other differences – melt flow is located in thin annular cylindrical gap, which resists flow in meridional plane, and walls of container are good conductors. So, in this equipment Lorentz force has r, φ and z components (in cylindrical coordinate system). Buoyancy force have z component. Both forces acts on the melt and defines melt flow in meridional (vertical plane) and azimuthal direction – $v(v_r, v_\varphi, v_z)$. Flow in meridional plane is generated by Lorentz and buoyancy forces, in azimuthal direction – only by EM forces. For representative values of simulation parameters see table 2.

3. Mathematical models and parameters of the equipment

Maxwell equations in quasi-stationary approximation were used to determine Lorentz force acting on melt [3]. Incompressible fluid flow calculation is described by Navier-Stokes equation:

$$\rho\left[\frac{\partial \vec{v}}{\partial t} + (\vec{v}\nabla)\vec{v}\right] + \nabla p - \eta\Delta\vec{v} = \vec{f}^{L} + \vec{f}^{B} \qquad (1)$$

$$\nabla \cdot \vec{v} = 0 \qquad (2)$$

where, p is pressure, η- viscosity, ρ – density, f – force density [4].

Right side terms f in equation (1) are Lorentz force density

$$\vec{f}^{L} = \frac{1}{2} Re\left[\vec{j} \times \vec{B}^{*}\right] \qquad (3)$$

and buoyancy forces

$$\vec{f}^{B} = -\rho(T)\vec{g} = -\rho_0 \vec{g}(1 - \beta(T - T_0)), \qquad (4)$$

where T is temperature, β – thermal expansion coefficient, T_0 – reference temperature, ρ_0 – density at reference temperature.

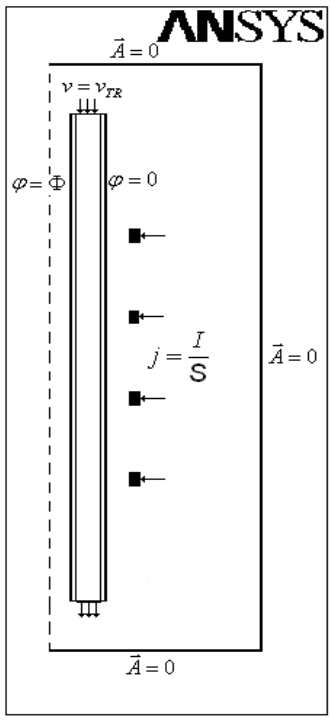

Fig.2. Applied boundary conditions and sources in axisymmetric plane.

Temperature field is determined by solving heat transfer equation:

$$\rho c_p \left[\frac{\partial T}{\partial t} + \nabla (T\vec{v}) \right] = \lambda \Delta T + q \,, \tag{5}$$

where c_p – specific heat capacity, λ – heat conductivity, Δ – Laplace operator, q – Joule heat density:

$$q = \frac{j^2}{2\sigma} \,. \tag{6}$$

Characteristic dimensionless numbers for this system are described in paper [1]. Magnetic field induced by melt flow can be neglected, because magnetic Reynolds number for data set 1 is about 10^{-9}.

For flow calculation laminar model can be used and inertial effects can be neglected, because Reynolds number does not exceed 1. Shielding effect of outer shell can be important at high frequencies, because skin layer depth at 100 kHz is 1.1 mm, which is smaller than thickness of shell - 1.2 mm.

Tab. 2 . Possible parameter values and values for used data sets

Parameter	Possible value range	data set 1
Frequency, kHz	1 -100	10
Viscosity, Pa·s	0.1..100	0.1
Potential difference on shells, V	0..5	0.1
Transient flow velocity (uniform inlet profile), mm/s	0..20.0	-
Shell conductance	$10^6 – 10^7$ S/m	$2 \cdot 10^6$ S/m
Melt conductance	1..100S/m	10S/m
Current in inductor, kA	$10^{-1}..10^2$	3

Due to such force combination, complicated flow structure can appear both in the meridional plane and in the azimuthal direction. It is possible to let these components be similar or exceed each other by changing parameters. In practical technological applications (melt nozzle) transit flow must be taken into account, that is carried out by applying velocity distribution $v=v_{TR}(r)$ at upper end of concentric shell tube (figure 2). Different thermal boundary conditions were used on both shells – adiabatic condition on inner shell and radiation to infinity on outer shell:

$$q' = \sigma_B \varepsilon \left(T^4 - T_{out}^4 \right) \tag{7}$$

where q' – heat flux

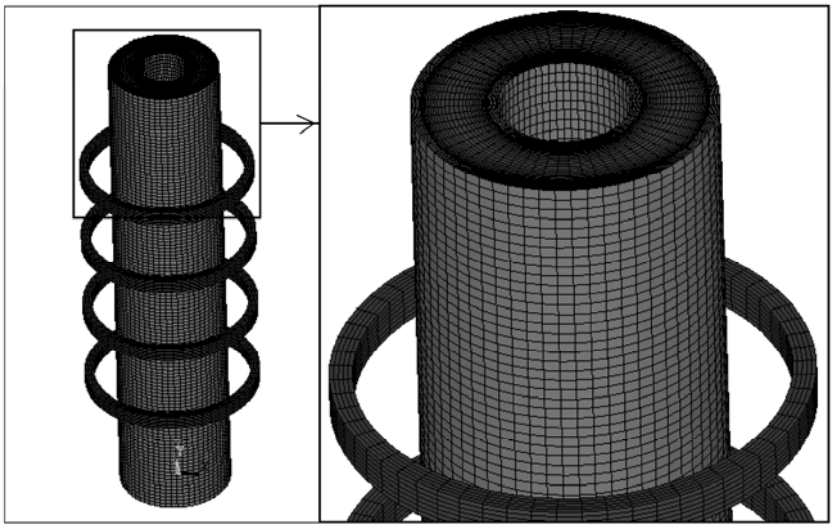

Fig. 3. Mesh of inductors, shells and melt domains. Air region is suppressed in that image. There are 30 fluid domain elements in radial direction with refinement near wall

density, σ_B – Stefan Bolzman constant, ε – emissivity coefficient, T_{out} – outer temperature.

Three main EM parameters, which can be varied, are the point of our interest – operating frequency, potential difference between shells and inductor current. Melt flow velocities depend on these quantities and estimation of character of this dependence is one of this paper goals.

4. Numerical simulation

EM calculations are performed in ANSYS Classic using full 3D model (due to ANSYS specific, we cannot perform 2D axial symmetric analysis). ANSYS Low-frequency EMAG Quasi-stationary simulation was carried out.

All simulations were performed using uniform mesh, generated using ANSYS Parametric Design Language (ADPL). Full 3D model for EM calculation contained approx. 350 thousands elements. Mesh of inductors, shells and melt domains is shown in figure 3.

Stationary HD and thermal calculations are performed in ANSYS CFX in 3D for full model. Mesh for HD calculation contained approx. 100 thousands elements.

5. Results

In weak conducting melt (oxides) furnaces, melt flow is often determined by buoyancy forces instead of Lorentz forces, which dominates in metallurgic equipment. Melt flow in meridional plane is determined by curl of forces acting (conservative forces in closed domain would not generate flow):

$$\left(\nabla\times\vec{f}^{\,T}\right)_{\varphi}=\left(\nabla\times(\vec{f}^{\,L}+\vec{f}^{\,B})\right)_{\varphi}=\frac{\partial f_r^L}{\partial z}-\frac{\partial f_z^L}{\partial r}-\frac{\partial f_z^B}{\partial r}. \qquad (8)$$

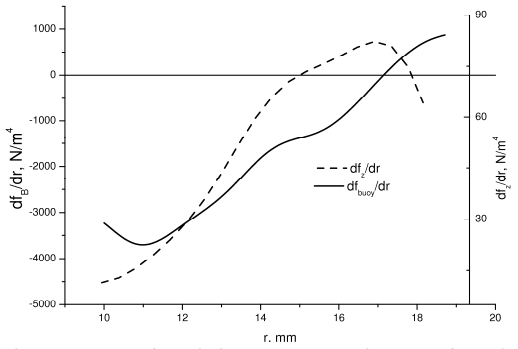

Fig. 4. Curl of buoyancy force density (left scale) comparison with curl of radial Lorentz force density (right scale) distribution along radius in melt in front of inductor section (data set 1)

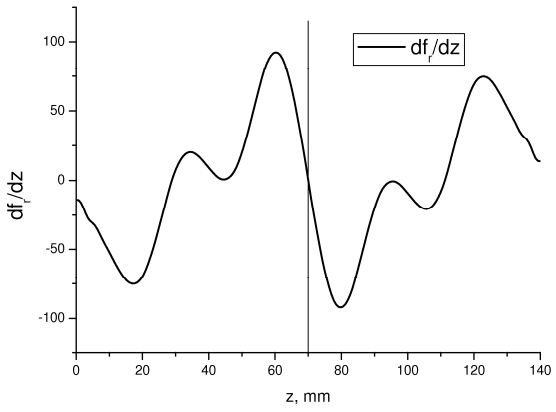

Fig. 5. Curl of axial Lorentz force density along height of melt domain at near inner shell (data set 1)

Figure 4 shows comparison of second and third term on right side of equation (7), figure 5 shows first term on right side of equation (7) – distribution is antisymmetric against middle plane of system due to phase shift π between upper

Table 3. Heat amount generated in different parts of the system (data set 1 in Table 2).

Part of system	Total heat amount, W
Outer shell	8948.4
Melt	7.2
Inner shell	632.9

two and bottom two coil current. It is obvious that curl of buoyancy force is two orders of magnitude higher than other terms in equation (7) - in this physical parameter range flow in meridional plane is mainly determined by buoyancy force.

Flow in azimuthal direction is determined by magnitude of force f_φ, while flow pattern can be closed.

Obtained electromagnetic results show that heat generated in melt is negligible if compared to heat generated in shells – this is due to induced currents in good conducting shells. Largest amount of heat appears in outer shell – it is about 15 times higher than heat in inner shell and about 1300 times higher than in melt. Heat generation at data set 1 in different parts of system is shown in table 3.

Figure 6 shows temperature field in melt and shells obtained without transit flow and corresponding flow streamlines. In this case relatively fast azimuthal flow does not change temperature field much (comparing to field obtained without motion of fluid), because streamlines are enclosed circles. It means that azimuthal flow could be insufficient for good stirring of melt, if axial flow is insufficient. In figure 6 streamlines of this flow are shown – it is visible, that flow in azimuthal direction is more intensive (~1.8 mm/s), while flow in, meridional plane is weak (~ 0.4 mm/s).

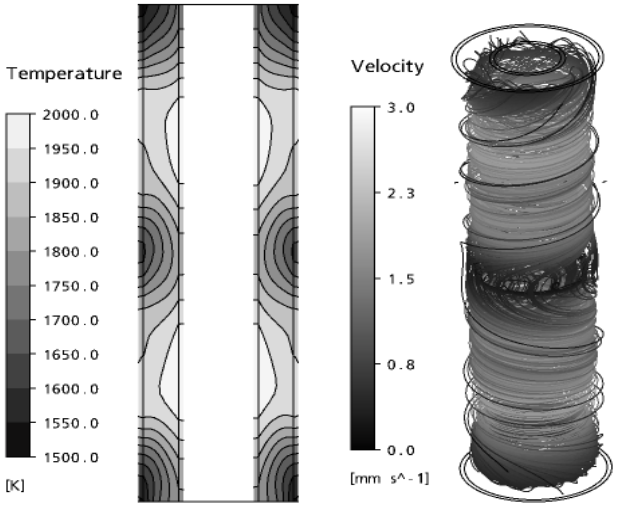

Fig. 6. Temperature field in melt and shells obtained used data set 1 (left), corresponding flow streamlines (right) without transit flow

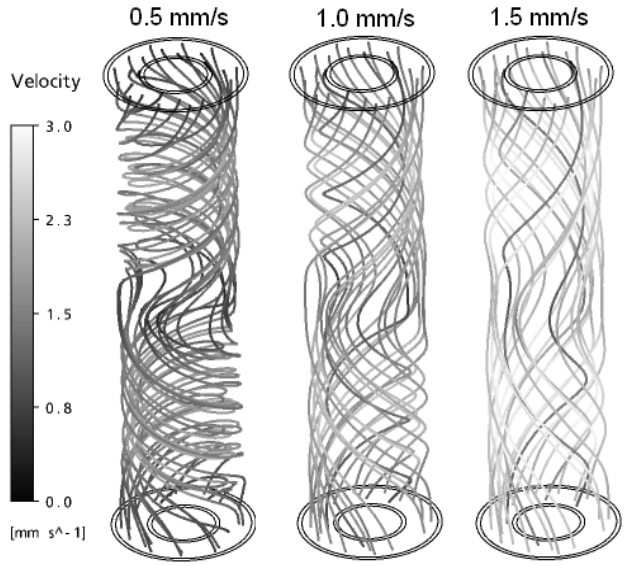

Fig. 7. Streamlines obtained with different transit flow velocities

For transit flow static temperature (1800 K) at inlet was applied at different inlet flow velocities. Curl flow appears with different angle of streamlines (figure 7), but buoyancy generated meridional flow is destructed by transit flow – more intensive meridional flow is necessary for complicated character of fluid motion. It is also obvious in figure 8, where temperature fields at different transit flow velocities are shown. Faster transit flow displaces temperature maximum points forward, also temperature is lower at highest transit flow values.

Figure 9 and figure 10 shows temperature distribution over radius in meltat two locations - 10 mm below lowest inductor section and at outlet correspondingly. In figure 9 temperature is maximal at 1.0 mm/s transit flow, because for faster flow local temperature minimum from central part of system is transmitted to observed location (see figure 8). It is also obvious that at outlet temperature are lower – melt cools down. For lower transit flow velocity values shape of temperature distribution between these two locations changes less,

than for faster transit flow. Total temperature range (difference between max and min) at outlet for lower transit flow is less – temperature distribution is more uniform. But for better homogenization more intensive flow in meridional plane should be achieved – it could make temperature more uniform at outlet.

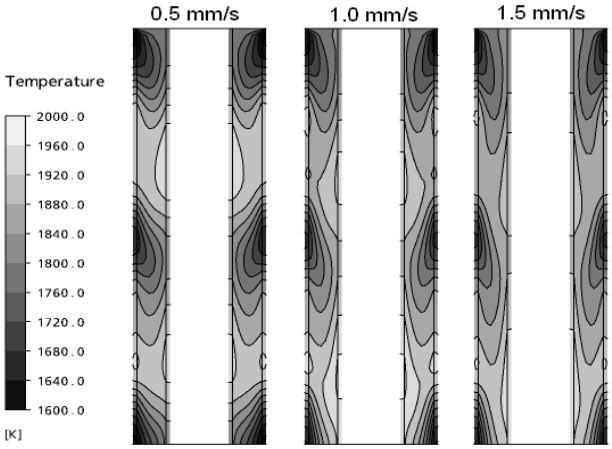

Fig. 8. Temperature field in melt and shells obtained with different transit flow velocities, temperature at inlet 1800 K

Conclusions

Simulations show, that previously used parameter range [1] is not suitable for experimental purpose, because heat generated in parts of equipment is too large. From obtained results we can conclude, that flow in meridional plane is estimated mainly by buoyancy force, in azimuthal direction – by Lorentz force. Highest flow velocities in meridional plane could stir melt better, while azimuthal flow does not change temperature field much. Experimental verification of obtained results is necessary for further work.

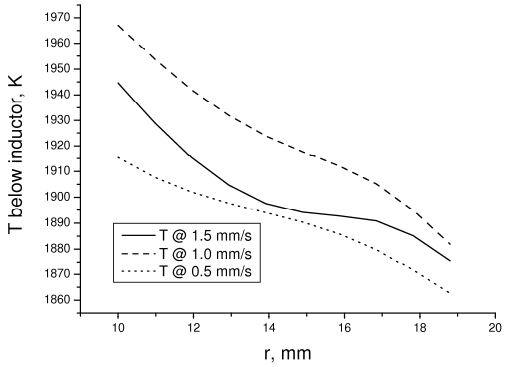

Fig. 9. Temperature distribution over radius 10 mm below lowest inductor section at different transit flow velocities.

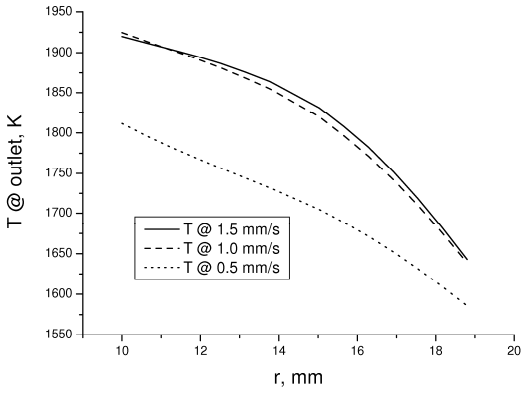

Fig. 10. Temperature distribution over radius at outlet at different transit flow velocities

References.

[1]. A. Jakovics, V.Geza, B.Halbedel. *Weak conducting material melt flow in crossed EM fields.* Przegląd Elektrotechniczny. 2008. (Accepted).
[2] A. Umbrashko, E. Baake, B. Nacke, A. Jakovics. *Modeling of the turbulent flow in induction furnaces*. Metallurgical and materials transaction B – 2006, vol. 37B, pp. 831 – 838
[3] John David Jackson. *Classical Electrodynamics*. 3rd edition. Wiley. 1998. pp.195-381.
[4] L.D.Landau,E.M. Lipschitz. *Hydrodynamics*. Nauka. Moscow. 1986. pp. 71-222.

Authors

Prof. Dr.-Phys. Jakovics, Andris;
Geza, Vadims
Fakulty of Physics and Mathematics
University of Latvia
Zellu str. 8, LV-1002 Riga, Latvia
E-mail: ajakov@latnet.lv

Prof. Dr.-Ing. Halbedel, Bernd
University Ilmenau,
Gustav-Kirchhof Strasse – 6,
D-98684, Ilmenau, Germany
E-mail: bernd.halbedel@tu-ilmenau.de